Biodegradation of bi-labelled polymer-coated rare-earth nanoparticles in adherent cell cultures.

Ziyao Liu[1], Alberto Escudero[2,3], Carolina Carrillo[4,5] , Indranath Chakraborty[1], Dingcheng Zhu[1], Marta Gallego[4], Wolfgang J. Parak[1,4*], Neus Feliu[1*]

[1]Center for Hybrid Nanostructures (CHyN) and Fachbereich Physik, Universität Hamburg, Hamburg, Germany

[2] INM – Leibniz Institute for New Materials. Campus D2 2. D-66123 Saarbrücken, Germany.

[3]Departamento de Química Inorgánica and Instituto de Investigaciones Químicas (IIQ), Universidad de Sevilla and Consejo Superior de Investigaciones Científicas (CSIC), Calle Américo Vespucio 49, E-41092 Seville, Spain.

[4]CIC Biomagune, San Sebastian, Spain
[5]Centro Singular de Investigación en Química Biológica y Materiales Moleculares (CiQUS) y Departamento de Física de Partículas, Universidad de Santiago de Compostela, Santiago de Compostela, Spain
[*]corresponding authors: wolfgang.parak@uni-hamburg.de, nfeliu@physnet.uni-hamburg.de

TOC

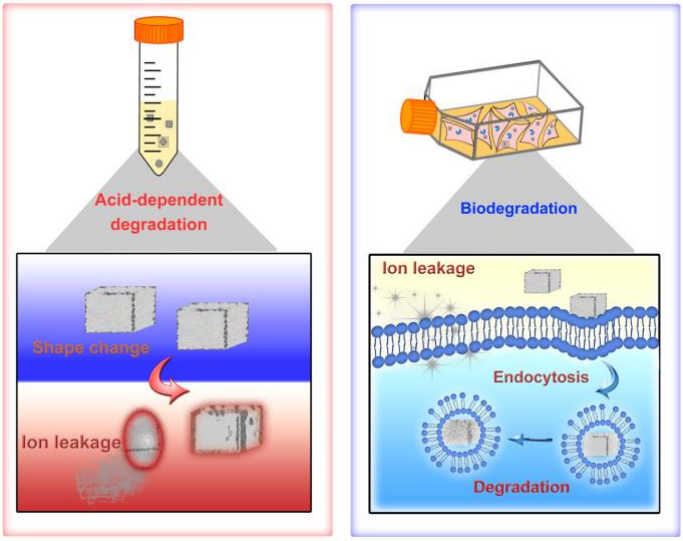

Abstract

The fate of polymer-coated Eu- and Bi-doped $GdVO_4$ nanoparticles of cubic shape upon cellular internalization was investigated. After endocytosis by cells, the cubic Eu- and Bi-doped $GdVO_4$ nanoparticle cores partly dissolved and were reshaped to rounded structures, which in control experiments could be ascribed to the acidic conditions present in endosomes/lysosomes. With

ongoing time, there was significant reduction of the amount of internalized nanoparticles *per* cell due to proliferation. This was of higher extent than nanoparticle exocytosis. Data of the study are compatible with the scenario that endosomal/lysosomal enzymes may partly digest the polymer shell around the nanoparticle cores, with enhanced exocytosis of the polymer fragments as compared to the nanoparticle cores.

Introduction

Nanoparticles (NPs) may be endocytosed and exocytosed by cells at *in vitro* level, and incorporated and excreted by tissues at *in vivo* level.[1-7] In the context of biological environment NPs need to be considered as hybrids comprising different components, such as the NP core, the NP surface coating, and the corona of adsorbed biological molecules such as proteins, counter ions, *etc.*[8] The biological fate of the respective components of hybrid NPs can be different.[9-14] In the following focus will be given on inorganic NP cores and organic surface coatings. Once exposed to different biological environments the NPs may be degraded, facilitated for example by acidic pH and presence of digestive enzymes.[15] The different components of the NPs thereby can undergo different fate. The inorganic NP cores can start to dissolve[16-22] and also reshaping has been reported.[17, 23-26] The organic surface coating around the NPs may desorb due to displacement by other molecules,[27-29] or may be enzymatically degraded.[30-36] Also adsorbed proteins may desorbed/displaced,[11, 37-42] and there may be enzymatic degradation.[43-45]

One way of following the fate of the different NP components upon cellular internalization is based on multiple labelling.[8, 46] By tracing of the different labels, the different NP components can be individually monitored. NP components may possess intrinsic properties that can act as label, *e.g.* fluorescence of the NP cores, different elements that can be detected by elemental analysis, *etc*. Alternatively, a large variety of labels can be attached to the different NP components, such as fluorophores, radiolabels, *etc*. Based on such multi-labelling studies, the fate of the different components of NPs once exposed to biological environment has been investigated. Details however depend on the respective NP structure. Thus, in order to obtain a more comprehensive picture, still more studies of different NP systems are needed.

In the present work intracellular degradation of polymer-coated Eu- and Bi-doped $GdVO_4$ NPs was investigated, focusing on both, degradation of the polymer shell and of the inorganic NP cores. While the NP cores were intrinsically fluorescent due to the Eu-doping and could be excited in the near ultraviolet region due to the presence of Bi,[47] the polymer coating based on polyacrylic acid (PAA) was labelled with organic fluorophores, *i.e*. fluoresceinamine (FA). Due to their composition, the NP cores also could be detected by elemental analysis (Eu, Bi, Gd). In this way, detection of the different NP components was possible by two complementary methods, fluorescence and elemental analysis. Emphasis was given on the following points. 1) In case the amount of (degraded) NPs *per* cell decreases over time, this may be due to exocytosis,[48] but also due to splitting of the NPs upon cell proliferation.[11, 49] Here, the role of proliferation was investigated quantitatively. 2) Degradation may release fragments of the organic surface coating from the NP cores.[11] Here, the kinetics of the intracellular concentration of several distinct components of the NPs (*i.e.* Eu, Bi, fluoresceinamine-labelled PAA) was comprehensively studied.

Results and Discussion

Synthesis and basic characterization of the NPs

PAA coated Eu- and Bi-doped $GdVO_4$ NPs were synthesized as described in previous work by one-pot synthesis with polymer functionalization (*i.e.* PAA coating). (REF 47) For degradation measurements concerning the PAA shell, PAA was labelled with FA and these NPs were termed FA-NPs. As shown by transmission electron microscopy (TEM), the inorganic cores of the NPs displayed well-defined cubic shape with d_c = 44 ± 6 nm diagonal length (n = 150 NPs, side length L_c = 32.9± 4.14 nm; see Figure 1 and the Supporting Information (SI)). This is in the same range as the hydrodynamic diameter of the NPs as dispersed in water, which was determined by dynamic light scattering (DLS) to be 33 ± 1 nm and 55 ± 1 nm from the number- and intensity distribution, respectively (see Figure SI-2.2.1). The zeta potential of the NPs in water at pH 6.5 was ζ = -32 ± 2 mV, provided by the negative charge of PAA. The fluorescence spectra showed the typical peaks due to Eu(III) and FA fluorescence (*cf.* Figure SI-2.4.1). Energy-dispersive X-ray spectroscopy (EDX) analysis further revealed homogenous distribution of Eu, Bi, and Gd in the NPs (see Figure SI-3.5.17). The concentration of the NPs was given in terms of mass concentrations C_{NP} [µg/mL], as determined by weighting of NP powder after solvent evaporation in an oven at 60 °C. For low concentrations the detection limit of the inductively coupled plasma mass spectrometry (ICP-MS) set-up was reached and thus low elemental concentrations C_{Eu}, C_{Bi}, and C_{Gd} were affected by a significant error.

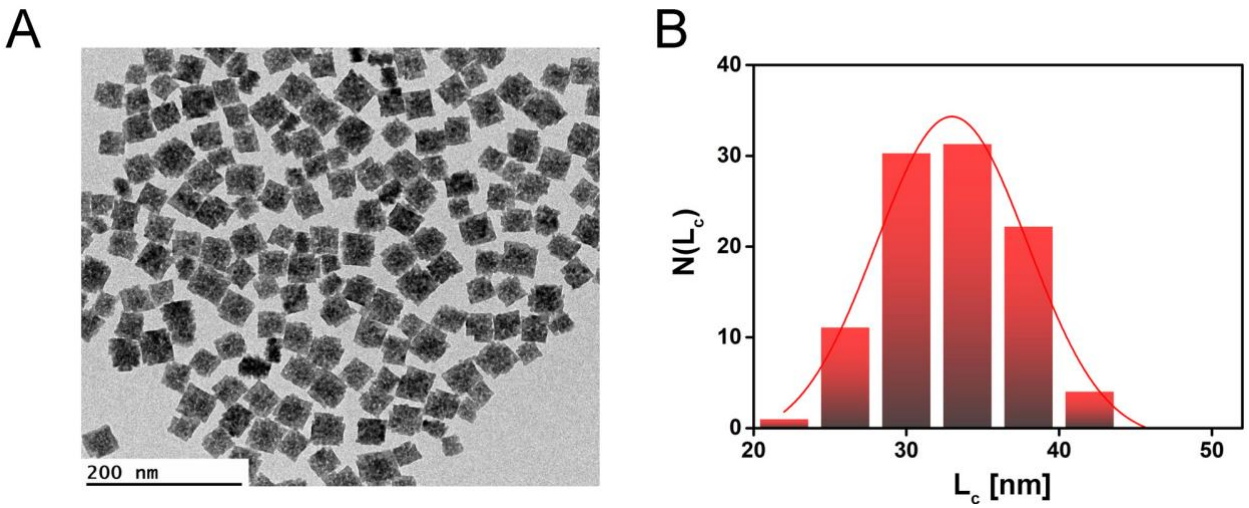

Figure 1. *Transmission electron microscopy (TEM) image of the NPs and the corresponding distribution of the side length L_c.*

NP degradation upon different incubation conditions

In order to emulate uptake of the NPs by cells, which involves acidic pH conditions as present in endosomes/lysosomes,[50] and a temperature of 37 °C as used for cultivating cell lines, potential

pH- and temperature-dependence of the degradation of the NPs was investigated. Rare earth metals for example have been reported to (partly) dissolve in acid buffer.[51-52] To evaluate acid-dependent degradation of the inorganic cores, three different pH conditions were chosen: (i) pH = 3.5 (citric acid–Na_2HPO_4), (ii) pH = 5 (citric acid–Na_2HPO_4), and (iii) either pH = 7.4 (citric acid–Na_2HPO_4) or pH = 6.3 (MilliQ water). To further investigate the influence of temperature, experiments were carried out either at room temperature (RT) or at T = 37 °C. Time dependent fluorescence measurements demonstrated that the Eu fluorescence of the NPs immersed in the different buffers decreased over time. At pH 3.5 the Eu fluorescence drastically decreased over time. pH 5 buffer caused a comparatively lower decrease of the Eu fluorescence, whereas the fluorescence intensity remained largely constant at pH = 7.4 buffer (*cf.* Figure SI-3.2.2). Higher temperature (37 °C *versus* RT) intensified the decrease of Eu fluorescence. Interestingly, the decrease of Eu fluorescence was also concentration-dependent. For concentrations $C_{NP} \gtrapprox 1$ mg/mL, the time-dependent reduction in Eu fluorescence was inhibited upon increasing the NP concentration (*cf.* Figure SI-3.2.1). The most likely explanation for this phenomenon is agglomeration of the NPs at high NP concentrations, leading to sedimentation of the NPs, and thus resulting in a reduced number NPs in the light path of the fluorimeter. Sedimentation of the milkish-white NP solution could be seen by the naked eye, and thus the solutions were mixed with a pipette before measurements. The same effect was also observed for FA dissolved in the different buffers. For FA concentrations $C_{FA} \gtrapprox 1$ μg/mL (this value depended on the pH of the buffer solution), FA fluorescence decreased with raising FA concentrations (*cf.* Figure SI-3.2.3). Due to the color of FA, the sedimentation of FA could also be seen by the naked eye. Thus, in the discussion of time- and pH-dependent fluorescence of Eu and FA also concentration dependence needs to be taken into account. Therefore, incubation experiments of cells with NPs were carried out at different NP concentrations.

While the NPs were colloidally stable in MilliQ water, *i.e.* had a hydrodynamic diameter d_h similar to the side length L_c of the cubic cores (*cf.* Figure SI-2.2.1), DLS measurements showed that the NPs severely agglomerated at pH 3.5 (*cf.* Figure SI-3.3.1). Agglomeration reduced over time, which might be due to partial dissolution of the NP cores. However, the PAA shell largely remained around the NP cores, as they kept their negative zeta-potential over time (*cf.* Figure SI-3.3.2). For pH 5 there was much less agglomeration, which also did not change over time, while there was no agglomeration in pH=6.3 (Milli-Q water, *cf.* Figure SI-3.3.1).

In order to analyze dissolution of the NP cores at pH 3.5 (only this pH value was used, as the change in fluorescence and size was the most obvious at this condition), NPs were incubated in pH 3.5 buffer at 37 °C for up to 30 days. After different incubation times, ions and small NP fragments released from the NPs were separated from the NPs by ultrafiltration and were quantified by ICP-MS.[53] The amount of Eu, Bi, and Gd released over time from the NPs is shown in Figure 2. Data clearly indicated that there was time-dependent release of the different elements, which demonstrated that the NP cores partly dissolved. However, the amount of released atoms was small as compared to the total amount of atoms in the NPs. Thus, there was

some release of atoms from the NP surface, but clearly no complete NP dissolution. Release of Eu and Gd was found to be faster than the one of Bi. Gd and Eu are both rare earth elements and thus were expected to show similar chemical behavior. Bi in contrast belongs to a different family of elements and thus possible $BiVO_4$ or Bi-rich clusters might be less soluble than $EuVO_4$ or $GdVO_4$. EDX data indicated that within the experimental error the Eu:Bi:Gd ratio in the NPs remained constant over time (*cf*. Figures SI-3.5.19 and SI-3.5.20). While ICP-MS data indicated higher release of Gd and Eu from the NPs (*cf.* Figure 2B), this release only made up for a small percentage of the total atomic content of the NPs. The absolute NP composition remained almost constant over time.

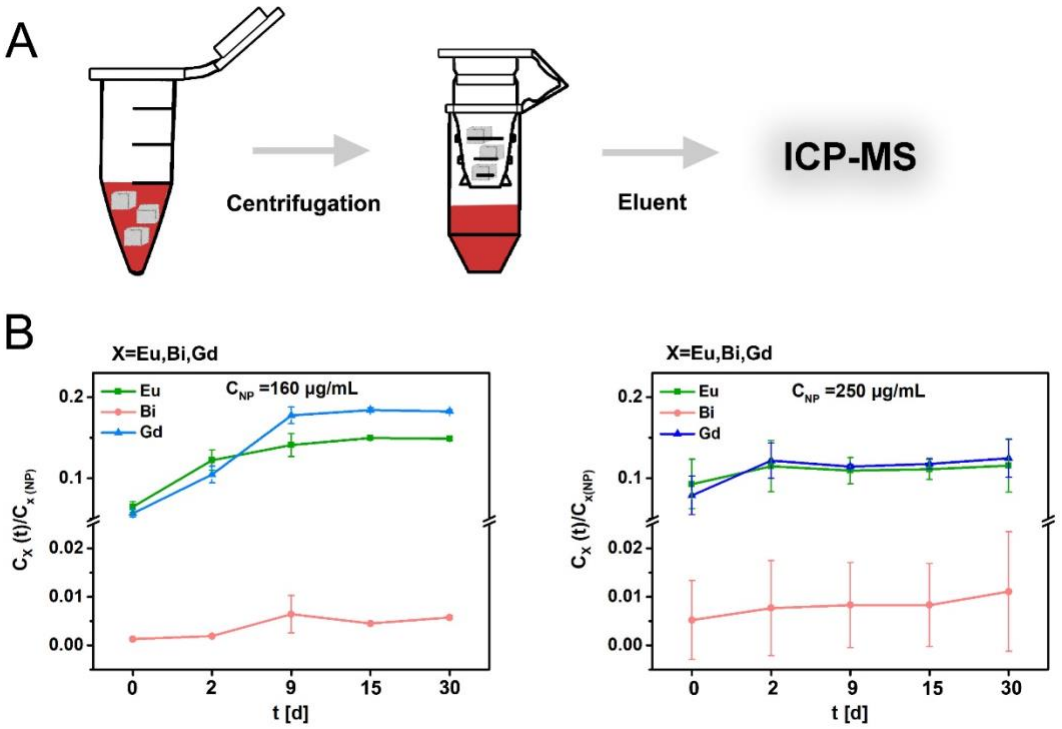

Figure 2. *(A) Schematic illustration for probing release of atoms/fragments from the NPs upon incubation at pH 3.5 at 37 °C. (B) The elemental concentrations of released atoms/fragments* C_{Eu}, C_{Bi}, *and* C_{Gd} *in the eluent were determined by ICP-MS. The amount of released atoms over time was normalized to the initial concentration of atoms in the NPs before elution and is plotted as* $C_X/C_{X(NP)}$ *(X = Eu, Bi, Gd). Data points correspond to mean values and standard deviations of n=3 measurements. The data are taken from Table SI-3.4.1.*

The ICP-MS data allowed for quantifying degradation of the NP cores in terms of released atoms per NP, but they did not provide structural information. Therefore, TEM analysis of the NPs after having been exposed to the different incubation conditions was performed (*cf.* Figures SI-3.5.3 - SI-3.5.15). Figure 3(A) shows the deformation of the cubic-shaped NP cores over time at pH 3.5. In contrast, at pH = 6.3 (MilliQ water) the NPs retained their cubic shape. The apparent deformation of cubic shape at acidic buffers encouraged us to study the shape evolution quantitatively. For this reason, the TEM images were digitally analyzed by the software cell

profiler and Matlab (see the SI for detailed information). Attempts were made for extracting various parameters for the different NPs, such as the cross section area of the NPs, their perimeter, eccentricity, extent, form factor, solidity, Z-factor, compactness, and corner angle.[54-56] More than 100 NPs were analyzed for each condition. However, only the corner angle α_{NP} clearly manifested the loss of cubic shape over time (*cf.* Figure SI-3.5.16), and thus the corner angle was used as quantifier. For the sharp edge of a cube α_{NP} is 90°, raising to α_{NP} = 180° for a flat surface. The more rounded the edges become, the more α_{NP} goes from 90° to 180°. The data in Figure 3 show a steep rise of α_{NP} in case the NPs were immersed in acidic buffer, whereas α_{NP} remained constant over time at pH=6.3 (Milli-Q water). Increasing temperature from RT to 37 °C did not accelerate loss of cubic shape. Most importantly, the $\alpha_{NP}(t)$ data also provide information about the kinetics. After around 2 weeks there was no further shape change.

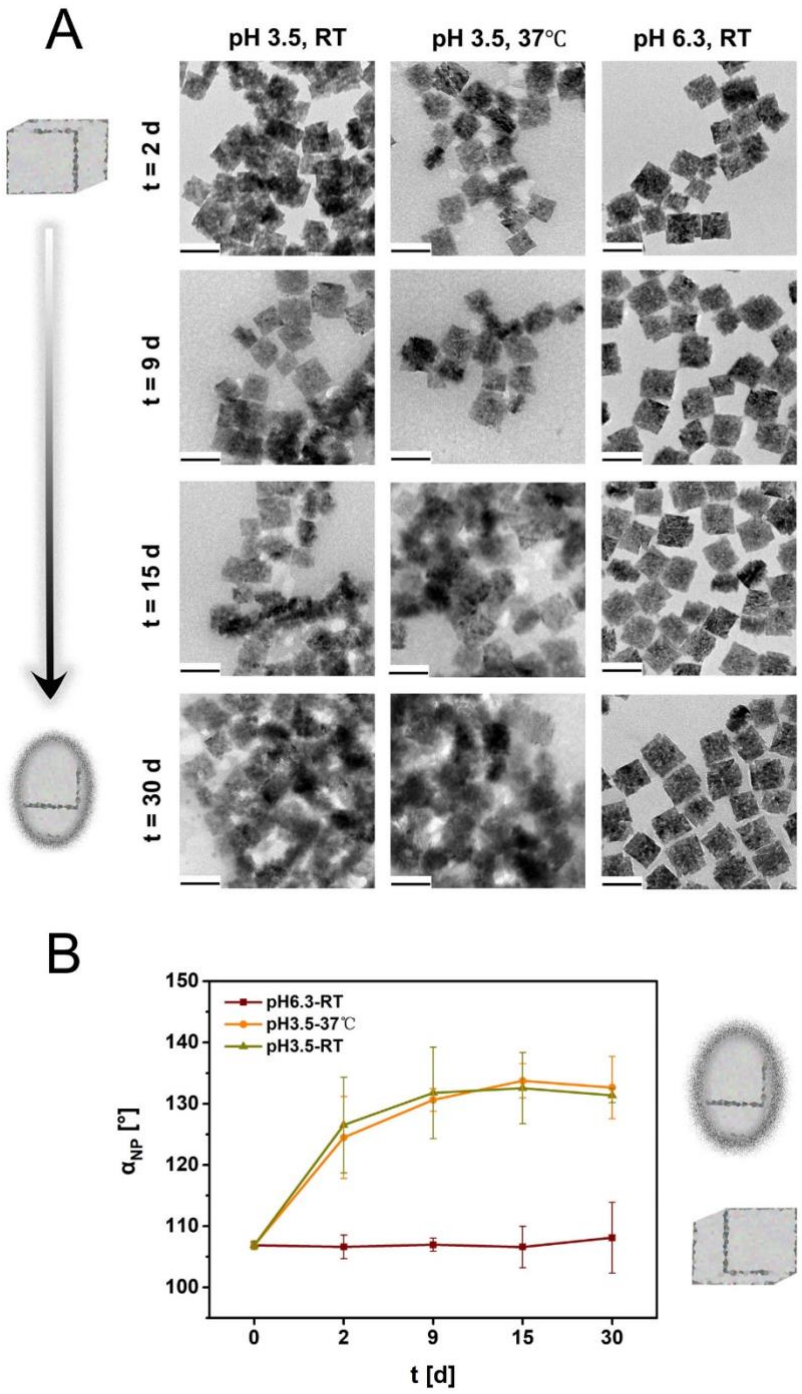

Figure 3*. (A) TEM images of NPs after incubation in different conditions. t indicates the incubation time. (B) Corner angle α_{NP} as calculated from TEM images.*

As mentioned before, EDX spectroscopy was performed during the TEM measurements (*cf*. Figures SI-3.5.17 and SI-3.5.18), which gave information about the amount and location of Eu, Bi, and Gd inside the NP cores. Data revealed that Eu, Bi, and Gd were homogeneously distributed in the NP cores for the different incubation conditions, and their ratio within the experimental error

stayed constant (*cf.* Figures SI-3.5.19 and SI-3.5.20). Even though the amount of released atoms was low, there still was a massive loss of cubic shape.

NP endo- and exocytosis

Uptake and excretion of NPs due to endo- and exocytosis was monitored *via* flow cytometry and ICP-MS, see Figure 4. Concentrations of NPs hereby were in a range where there was no acute reduction in cell viability of the cells due to being exposed to NPs (*cf.* Figure SI-4.2.1), as there was negligible effect on cell proliferation (*cf.* Figure SI-4.2.2).

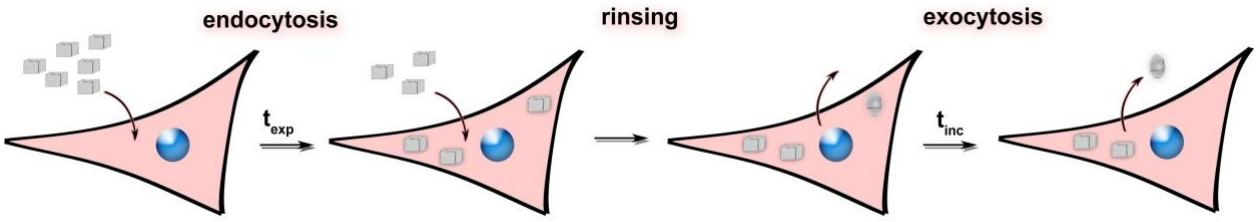

Figure 4. *Work flow for investigating the uptake and fate of NPs by cells. At time t = 0, cells were exposed to NPs at the concentration C_{NP} for the time t_{exp} in serum-supplemented medium. During this time, NPs were endocytosed by cells, which was quantified by flow cytometry or ICP-MS. At time t_{exp}, the medium with the remaining NPs was removed, cells were rinsed and fresh serum-supplements medium was added. The time point before and after washing was defined as $t_{inc} = 0^-$ and 0^+, respectively. The fate of the NPs inside cells was then observed upon continuous incubation for the period t_{inc}. The total time passed for the experiment at this point was $t = t_{exp} + t_{inc}$. During this ongoing incubation, NPs may have been degraded and exocytosed, as well as they were passed to daughter cells upon cell proliferation. The amount of remaining NPs inside cells was quantified by flow cytometry or ICP-MS.*

In Figure 5 the endocytosis experiments are presented. As well the flow cytometry (Figure 5B), as the ICP-MS (Figure 5C) data show a concentration- and time-dependent uptake of NPs. The concentration of the NPs remaining in the extracellular solution (Figure 5D) displayed no time-dependent reduction, which demonstrated that there were more NPs in solution than cells can incorporate, maintaining approximately constant the extracellular NP concentration during the incubation process.[57] The time-dependence in internalization was different in the flow cytometry and in the ICP-MS data. The ICP-MS data indicated that the longer exposure time t_{exp}, the more NPs in terms of elemental concentrations were internalized *per* cell (*cf.* Figure 5C for Eu und Gd; data for Bi are shown in Figures SI-6.1.1 and SI-6.1.2). In contrast, there was less NP fluorescence inside cells after 48 h than after 6 h and 24 h (Figure 5B), in both, the Eu- and the FA-channel. First of all, this highlighted the advantage of measuring NP internalization with different methods, as different methods are sensitive to various factors. Eu fluorescence of NPs in environment emulating endocytosed NPs (acidic pH, pH = 37 °C) was reduced over time (*cf.* Figures SI-3.2.2B, SI-3.2.1A, Figure SI-5.2.1A). Changes in the cristallinity and in the NPs structure and morpholoy

produced by NPs degradation at acidic pH (see Intracellular deformation of NPs section) may be responsible for the loose of Eu fluorescence with increasing incubation time, which is compatible with a less fluorescence in the Eu-channel after 48 h. There was also quenching of FA fluorescence over time of NPs in the environment mimicking the one of NPs within cells (acidic pH, pH = 37 °C), *cf.* Figure SI-5.2.1B (which is more relevant to the biological conditions than data recorded without cells in Figure SI-3.2.3, where there is rather slight fluorescence enhancement). There was less reduction of NP fluorescence in the FA- than in the Eu-channel after 48 h as compared to 24 h, which was in line with these findings. The data do not exclude that there might have been a loss of FA upon intracellular degradation of the NPs, followed by exocytosis of FA.

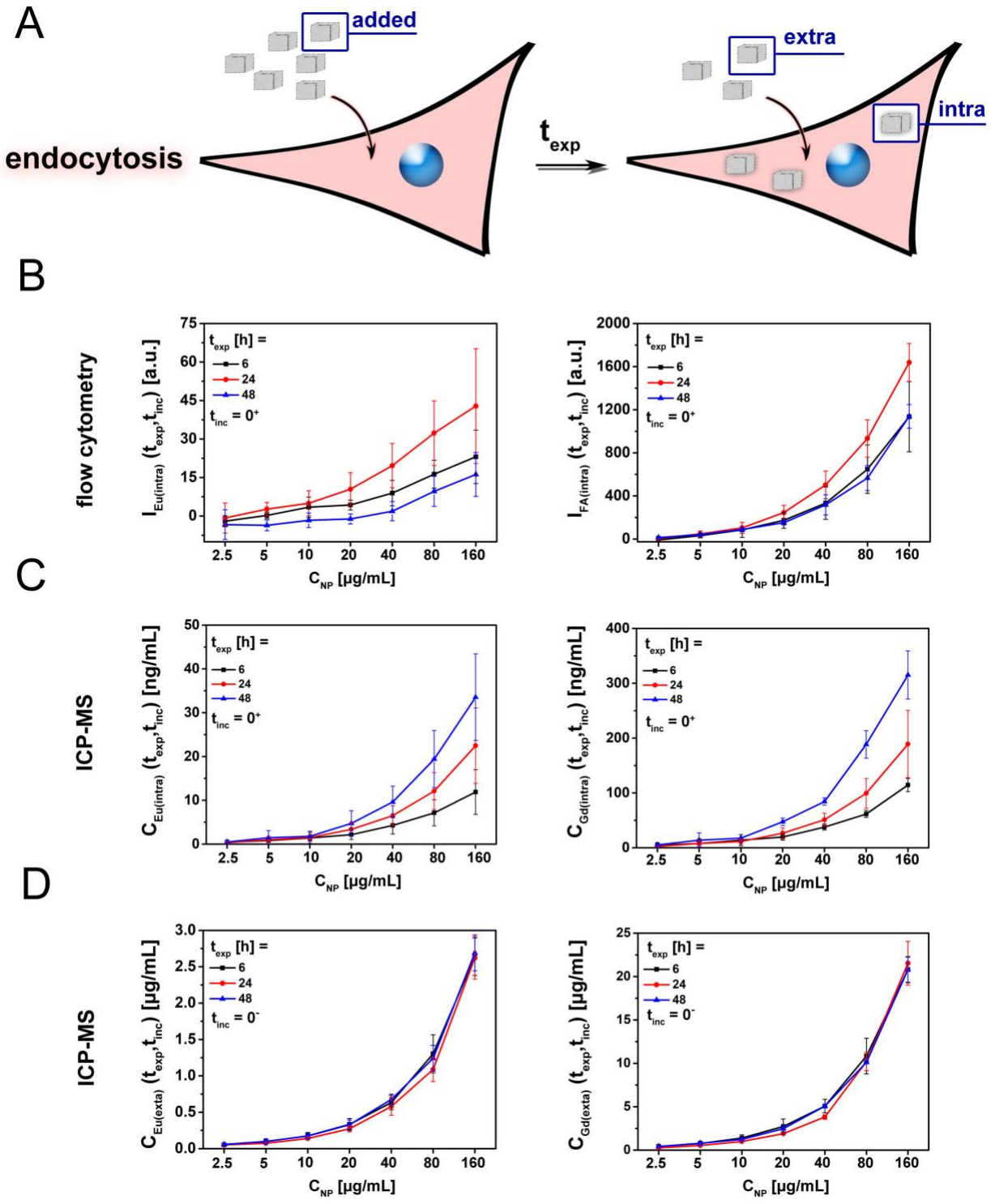

Figure 5. *(A) Quantification of the uptake of (B) FA-NPs and (C,D) NPs by Hela cells. Hela cells were incubated for the time t_{exp} with FA-NPs or NPs at concentration C_{NP} in serum-supplemented medium. (B) After removal of excess NPs in the supernatant (i.e. $t_{inc} = 0^+$), the mean Eu fluorescence $I_{Eu(intra)}$ and the mean FA fluorescence $I_{FA(intra)}$ per cell were determined by flow cytometry analysis. Data correspond to the mean value and standard deviation of n=3 measurements. The artificial "negative" intensity values at low NP concentrations were due to the offset correction of auto-*

fluorescence and indicated that for low concentrations intensities were below the quantifiable detection limit. (C) After removal of excess NPs in the supernatant (i.e. $t_{inc} = 0^+$), the cells were pelleted and the mass of Eu and Gd in the cell pellet was determined by ICP-MS (these data are very similar to the ones of Bi which are shown in Figure SI-6.1.1(A)). The "mass-concentrations" $C_{Eu(intra)}$ and $C_{Gd(intra)}$ of internalized Eu and Gd, respectively, were calculated by dividing the masses of Eu and Gd in the cell pellet by the volume of the cell culture medium above the cells, which could be compared directly with the concentration of added NPs C_{NP}. Data correspond to the mean value and standard deviation of at least n≥3 measurements. (D) After the exposure time t_{exp}, the NPs remaining in the supernatant (i.e. without rinsing, $t_{inc} = 0^-$) were analyzed by ICP-MS, resulting in the Eu and Gd concentration in the supernatant, which had the same volume as the cell culture medium above the cells. Data for Bi were similar to data for Eu and are shown in Figure SI-6.1.1(B). Data correspond to the mean value and standard deviation of at least n≥3 measurements.

In Figure 6 the loss of intracellular NPs, after having removed all residual NPs from the extracellular medium, is plotted over time. The fluorescence data (*cf.* Figure 6B) clearly showed a time-dependent decrease of intracellular NP-associated fluorescence. Fluorescence spectroscopy data as recorded on cell lysates demonstrated the same trend, *cf.* Figure SI-8.1.1. Flow cytometry is a single cell-based technique, in which the mean intracellular fluorescence *per* cell is determined. Apart from eventual quenching phenomena, reduction in fluorescence can be due to sharing of NPs by daughter cells upon cell proliferation (which in on the time scale of hours),[58] or by exocytosis of NPs.[11, 59] In order to cancel out NP dilution *via* proliferation, the intracellular fluorescence *per* cell was related to the number of cells at the beginning of NP exposure ($t_{inc} = 0^+$, Figure 6C). This was done based on the experimentally determined proliferation rate of cells (*cf.* Figure SI-4.3.1). This presentation is different to the one used Figure 6B, where the intracellular fluorescence *per* cell is related to the number of cells after having incubated cells with NPs for the time t_{inc}. If intracellular fluorescence was normalized to the initial number of cells, *i.e.* cancelling out proliferation-caused dilution of internalized NPs, then there barely was a time-dependent decrease in intracellular NP fluorescence, in particular for the Eu-channel (*cf.* Figure 6C). This suggested, that in particular for the NP cores (as quantified by the Eu fluorescence) there was little exocytosis. This result is in agreement with recent work from others.[60] There was some time-dependent decrease in the FA-channel, which would be compatible with the scenario that parts of the FA-labelled polymer shell were enzymatically degraded and fragments were exocytosed.[30] As exocytosis is size-dependent,[58] fragments of the polymer shell (as labelled by FA) would be faster exocytosed than the NP cores (as quantified by Eu inside cores). Note, that in previous work faster exocytosis of NP cores than of polymer fragments was found, which was attributed to NP agglomeration after partial loss of the polymer shell.[11] As in the present study the internalized NPs were already partly agglomerated (*cf.* Figure SI-3.3.1), this effect did not apply here, explaining the enhanced exocytosis of the fragmented polymer capping. Also in the ICP-MS data no strong time-dependent decrease of intracellular NP elements (Eu, Gd; data for Bi are shown in Figures SI-6.1.1 and SI-6.1.2) was observed, see Figure 6D. In the ICP-MS data the amount of intracellular Eu, Gd, and Bi was related to the number of initial cells ($t_{inc} = 0^+$), thus not taking NP dilution due to proliferation into account. The ICP-MS data (Figure 6D) were consistent with the

flow cytometry data, in which proliferation was disregarded due to normalization to the initial number of cells (Figure 6C). This confirmed that loss in NPs *per* actual number of cells was mainly due proliferation, and not due to exocytosis.

Apart from the time-decay of the intracellular NPs as quantified by flow cytometry and ICP-MS, also the raise in extracellular NPs was quantified, see ICP-MS data in Figure 6E. Of note, the ICP-MS data were mass-balanced, *i.e.* the sum of intracellular and extracellular NPs remained constant, no NPs were "lost", *cf.* Figure SI-6.1.4. Only at very low NP concentrations, there were significant errors due to the detection limit of ICP-MS. After removal of extracellular NPs, the reason for the increased NP concentration in the extracellular solution can be only due to exocytosis, but not due to proliferation (neglecting the error that some NPs may have stuck to the extracellular cell walls and were not removed during rinsing). Thus, despite the fact that cell proliferation was the main reason for the decreasing NP concentration in individual cells, there was also exocytosis of NPs. The amount of exocytosed NPs increased with time (t_{inc}). However, compared with the original amount of internalized NPs at $t_{inc} = 0^-$, the exocytosed NPs only accounted for a small fraction (Figure 6E). Accordingly, the majority of NPs remained inside endosomes/lysosomes, and exocytosis on the time scale of days was not capable of removing a large fraction of NPs from cells. Again, the main reason for reduction of the number of NPs *per* cell was due to proliferation. Data were also recorded under the presence of endocytosis/exocytosis blockers, such as chloroquine as inhibitor of the acidification of endosomes/lysosomes,[61-63] ammonium chloride as inhibitor of phagosome/lysosome fusion,[64-66] and pepstatin A as inhibitor of proteases.[67-68, 69] Data were recorded with flow cytometry (*cf.* Figures SI-5.3 and SI-5.4) and ICP-MS (*cf.* Figures SI-6.2.1 and SI-6.2.2). However, as blockers also effected cellular proliferation (*cf.* Figure SI-5.3C) the observed slowing down of the time-dependent concentration loss of intracellular NPs was most likely due to reduction of proliferation.

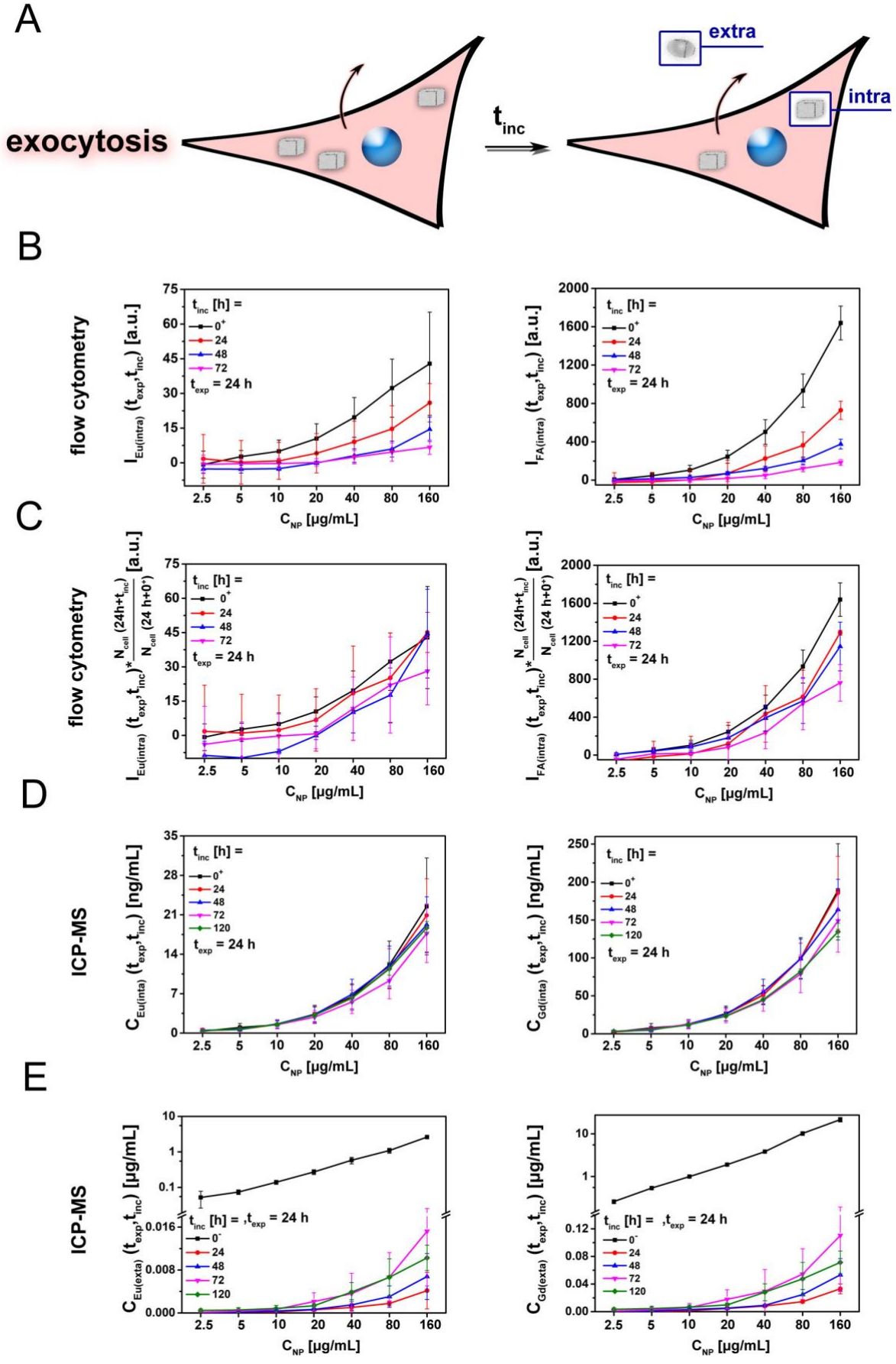
A
exocytosis
t_inc
extra
intra
B
flow cytometry
I_Eu(intra) (t_exp,t_inc) [a.u.]
I_FA(intra) (t_exp,t_inc) [a.u.]
t_inc [h] =
0+
24
48
72
t_exp = 24 h
C_NP [µg/mL]
C
flow cytometry
I_Eu(intra) (t_exp,t_inc)*N_cell(24h+t_inc)/N_cell(24 h+0+) [a.u.]
I_FA(intra) (t_exp,t_inc)*N_cell(24h+t_inc)/N_cell(24 h+0+) [a.u.]
D
ICP-MS
C_Eu(inta) (t_exp,t_inc) [ng/mL]
C_Gd(inta) (t_exp,t_inc) [ng/mL]
120
E
ICP-MS
C_Eu(exta) (t_exp,t_inc) [µg/mL]
C_Gd(exta) (t_exp,t_inc) [µg/mL]
t_inc [h] = ,t_exp = 24 h
0-

Figure 6. *(A) Quantification of the fate of (B) FA-NPs and (D;E) NPs by Hela cells. Hela cells were incubated for the time t_{exp} with FA-NPs or NPs at concentration C_{NP} in serum-supplemented medium. After removal of excess NPs in the supernatant (directly before removal: $t_{inc} = 0^-$; directly after removal: $t_{inc} = 0^+$), cells were incubated again for the time t_{inc}. (B) After washing of the cells, the mean Eu fluorescence $I_{Eu(intra)}$ and the mean FA fluorescence $I_{FA(intra)}$ per cell were determined by flow cytometry analysis. Data correspond to the mean value and standard deviation of n=3 measurements. The artificial "negative" intensity values at low NP concentrations were due to the offset correction of auto-fluorescence, indicating that for low concentrations intensities were below the quantifiable detection limit. (C) As cells growew during the period t_{inc}, the data from (B) were normalized by the ratio of cells before and after incubation, which is displayed in Figure SI-4.3.1. (D) After removal of excess NPs in the supernatant (i.e. $t_{inc} = 0^+$), the cells were pelleted and the mass of Eu and Gd in the cell pellet was determined by ICP-MS (these data were very similar to the ones of Bi which are shown in Figures SI-6.1.1(C)). The "mass-concentrations" $C_{Eu(itra)}$ and $C_{Gd(intra)}$) of internalized Eu and Gd, respectively, were calculated by dividing the masses of Eu and Gd in the cell pellet by the volume of the cell culture medium above the cells, and thus could be directly compared with the concentration of added NPs C_{NP}. Other representations of the same data are provided in Figure SI-6.1.2. Data correspond to the mean value and standard deviation of at least n≥3 measurements. (E) After the exposure time t_{exp}, the NPs remaining in the supernatant (i.e. without rinsing, $t_{inc} = 0^-$) were analyzed by ICP-MS. This yielded the Eu and Gd concentration in the supernatant, which had the same volume as the cell culture medium above the cells. The value at $t_{inc} = 0^-$ thus corresponded to the NPs in the supernatant which had not been internalized by cells, and the values for $t_{inc} > 0$ corresponded to the NPs which have been exocytosed to the cell medium. Data for Bi were similar to data for Eu and are shown in Figure SI-6.1.1(D). Data correspond to the mean value and standard deviation of at least n≥3 measurements. Note that for all the data shown in this figure the values for $t_{exp} = 24$ h and $t_{inc} = 0$ are the same which have been already displayed in Figure 5.*

<u>Intracellular deformation of NPs</u>

TEM was used to follow the structural evolution of the internalized NP cores. Note that the polymer surface did not provide sufficient contrast for being visualized with TEM. Figure 7 shows the time-dependent shape change of the NPs. Most of NPs were randomly distributed in intracellular vesicles (endosomes/lysosomes) just after internalization (t_{exp} = 6 h, $t_{inc} = 0^+$). There were still some non-internalized NPs attached to the outer cell membrane. With increasing time, the initial sharp edges of the cubic-shaped NPs became blunted. The NPs progressively lost their well-defined cubic shape and turned into irregular roundish structures. Eventually, the degraded NPs also formed large aggregates. In order to get quantitative results, the same method as applied for analysis the shape-change of free NPs (*cf*. Figure 3) was adopted. The time-dependent rise in the corner angle α_{NP} (*cf.* Figure 7) clearly showed the shape deformation over time. The results were in line with the evolution of the corner angle in acid buffer (*cf.* Figure 3B). This indicates that loss in NP shape was caused by the acidic pH inside endosomes/lysosomes.

It is important to point out that NPs did not completely dissolve, as it is also know from other materials such as silver.[70-71] While there was leaching of ions from the NP cores (*cf.* Figure 2), the liberated ions were still trapped inside the same endosomes/lysosomes as the NP cores. The released ions could not escape efficiently from endosomes/lysosomes, which maybe was also due to complexation of released ions by proteins. Thus, the ion concentration inside endosomes/lysosomes remained high enough to allow for regrowth of the NPs (*i.e.* super-saturation). Similar re-precipitation has been reported for other materials.[72] In this way, NPs would not have finally dissolved, but rather reshaping would have occurred, as it is also known from other NP materials.[16]

A

t_{exp} = 6 h
t_{inc} = 0^+ h

t_{exp} = 24 h
t_{inc} = 0^+ h

t_{exp} = 24 h
t_{inc} = 72 h

t_{exp} = 24 h
t_{inc} = 120 h

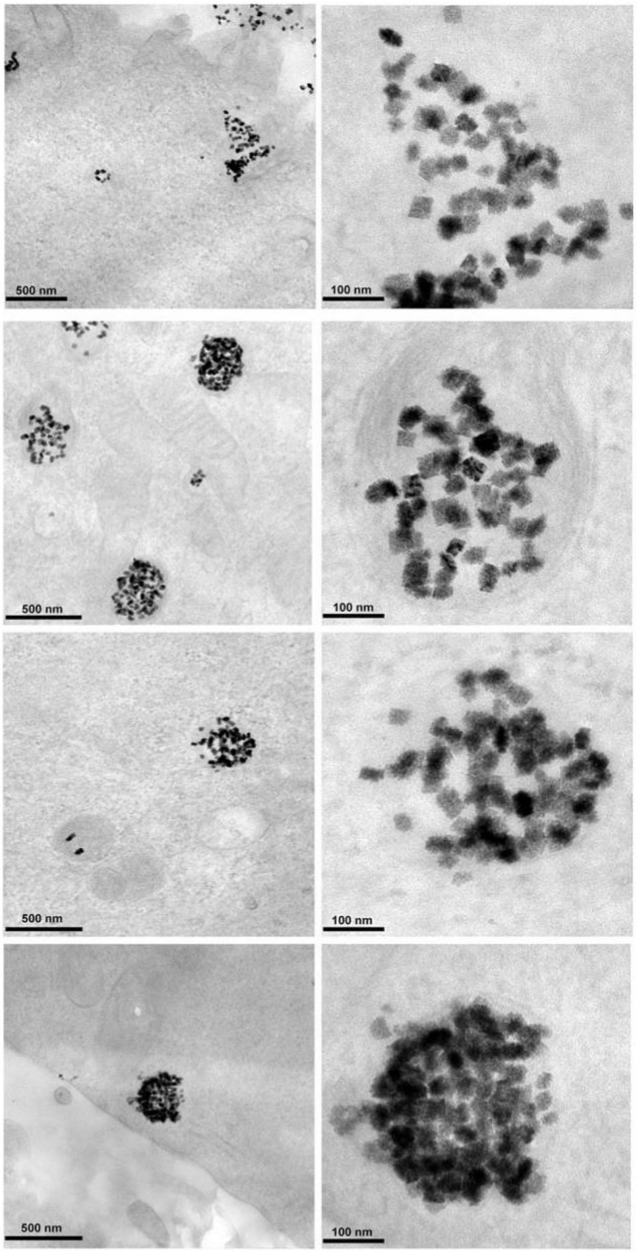

B

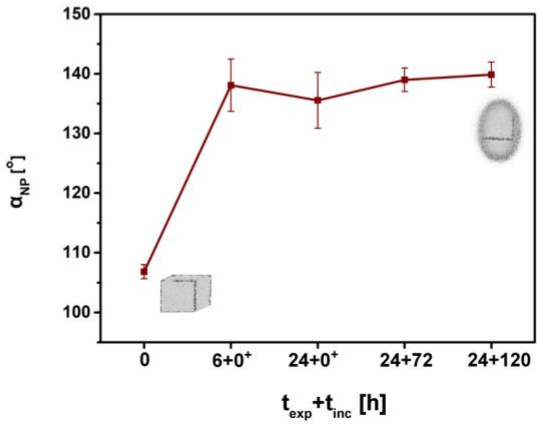

Figure 7. *(A) Cells had been incubated with NPs for the time t_{exp} at concentration C_{NP} = 160 µg/mL. After removal of NPs from the extracellular medium, the cells were incubated further for the time t_{inc}. Then TEM images of the cells after fixation were taken. Two addition data series are depicted in Figure SI-9.1.1. (B) Analysis of the time dependent corner angle α_{NP} as extracted from the TEM images. The full parameter set can be seen in Figure SI-9.1.6.*

Separation of the polymer shell from the NP core

For other NP systems, partial enzymatic degradation of the polymer shell and subsequent separation from NP cores has been reported.[11, 30-31] In the present study there is a massive data set about the time-dependent fate of the different NP compartments, as quantified by different methods: core- and shell- fluorescence quantified by Eu and FA-labelling, and elemental mass concentrations of different NP core elements (Eu, Gd, Bi) measured by ICP-MS. ICP-MS data were not affected by any quenching effect, but they only referred to elements present in the NP cores and did not provide information about the NP shell. The Eu- as well as the FA fluorescence used for quantifying NP cores and shells however were affected by fluorescence quenching, which was higher for the Eu fluorescence. In Figures SI-7.1.1 - SI-7.3.3, the ratios of the different quantifiers (fluorescence, elemental concentrations) are plotted. Due to quenching effects in fluorescence, a possible separation of the polymer shell followed by exocytosis from the NP cores was hard to quantify. Figures SI-7.3.2A,B suggests, that there was a stronger decrease of shell fluorescence (FA) as compared to core fluorescence (Eu), which would be compatible with partial release and exocytosis of the polymer shell. Our data however do not allow for solid quantification of this process, in particular as exocytosis accounts less for reduction of intracellular NP concentrations than proliferation. However, in previous studies with NPs of higher fluorescence this effect could be quantified.[11]

Conclusions

As there are many interconnected effects, it is difficult to make a solid quantification of intracellular NP degradation that includes the analysis of different NP compartments such as inorganic cores and polymer shells. For the case of polymer-coated Eu- and Bi-doped $GdVO_4$ NPs of cubic shape with side length side L_c = 32.9± 4.14 nm of the NP cores, the following conclusions could be drawn. Upon cellular internalization, there is a partial degradation of the NP cores, which however does not lead to significant dissolution, but rather to reshaping, resulting in loss of cubic shape. Emulation experiments in acidic pH suggest that this process is due to the acidic pH present in endosomes/lysosomes. On condition that no new NPs can be internalized (*i.e.* by removal of NPs from the extracellular medium), there is a time-dependent loss of NP concentration *per* cell. The dominating effect hereby is NP dilution due to cell proliferation, where NPs are split between daughter cells. Exocytosis also leads to the decrease of NP concentration per cell, which however has less impact than proliferation. Exocytosis data are compatible with the scenario that digestive proteins inside lysosomes partly degrade the polymer shell around the NP cores, which is exocytosed to a higher extent than the NP cores. Due to the low Eu-fluorescence of the NP cores,

and fluorescence quenching of both, Eu- and FA-fluorescence, this effect however could not be quantified.

Materials and Methods

Synthesis and Characterization. NP synthesis followed published protocols.[47] Characterization of the NPs was done by using transmission electron microscopy (TEM), dynamic light scattering (DLS), laser Doppler anemometry (LDA), inductively coupled plasma mass spectrometry (ICP-MS), UV/vis absorption, and fluorescence spectroscopy, all based on established protocols.[53] All protocols are described in detail in the SI. Degradation studies of the NPs were carried out in various media. Changes in the fluorescence spectra and hydrodynamic diameter were thoroughly investigated by incubation of the NPs in buffers with different pH value for different incubation times. Changes in NP properties were recorded by fluorescence spectroscopy and DLS.[53] Structural analysis for these samples was further performed by TEM, EDX, and ICP-MS. All protocols are described in detail in the SI.

Acknowledgements

ZL acknowledges a PhD fellowship from the Chinese Scholarship Council (CSC). The project was supported by the Deutsche Forschungsgemeinschaft (DFG grant PA 794/25-1). AE acknowledges the support of Prof. Tobias Kraus and Prof. Eduard Artz (INM, Saarbrücken) and the 6th Research and Technology Transfer Plan of the University of Seville (VI PPIT-US).

References

1. Bargheer, D.; Giemsa, A.; Freund, B.; Heine, M.; Waurich, C.; Stachowski, G.; Hickey, S.; Eychmüller, A.; Heeren, J.; Nielsen, P., The distribution and degradation of radiolabelled SPIOs and Quantum Dots in mice. *Beilstein Journal of Nanotechnology* **2015,** *6*, 111-123.
2. Mazuel, F. o.; Espinosa, A.; Luciani, N.; Reffay, M.; Borgne, R. m. L.; Motte, L.; Desboeufs, K.; Michel, A.; Pellegrino, T.; Lalatonne, Y.; Wilhelm, C., Massive Intracellular Biodegradation of Iron Oxide Nanoparticles Evidenced Magnetically at Single-Endosome and Tissue Levels. *ACS Nano* **2016,** *10*, 7627−7638.
3. Stepien, G.; Moros, M.; Pérez-Hernández, M.; Monge, M.; Gutiérrez, L.; Fratila, R. M.; Las Heras, M.; Menao Guillén, S.; Puente Lanzarote, J. J.; Solans, C.; Pardo, J.; de la Fuente , J. M., Effect of Surface Chemistry and Associated Protein Corona on the Long-Term Biodegradation of Iron Oxide Nanoparticles In Vivo. *ACS Appl Mater Interfaces* **2018,** *10*, 4548-4560.
4. Gilbert, B.; Fakra, S. C.; Xia, T.; Pokhrel, S.; Madler, L.; Nel, A. E., The Fate of ZnO Nanoparticles Administered to Human Bronchial Epithelial Cells. *Acs Nano* **2012,** *6* (6), 4921-4930.
5. Zhu, M. T.; Nie, G. J.; Meng, H.; Xia, T.; Nel, A.; Zhao, Y. L., Physicochemical Properties Determine Nanomaterial Cellular Uptake, Transport, and Fate. *Acc. Chem. Res.* **2013,** *46* (3), 622-631.

6. Chen, F.; Goel, S.; Valdovinos, H. F.; Luo, H.; Hernandez, R.; Barnhart, T. E.; Cai, W., In Vivo Integrity and Biological Fate of Chelator-Free Zirconium-89-Labeled Mesoporous Silica Nanoparticles. *ACS Nano* **2015,** *9* (8), 7950-9.
7. Sharma, V. K.; Siskova, K. M.; Zboril, R.; Gardea-Torresdey, J. L., Organic-coated silver nanoparticles in biological and environmental conditions: fate, stability and toxicity. *Adv. Colloid Interface Sci.* **2014,** *204*, 15-34.
8. Rivera Gil, P.; Jimenez de Aberasturi, D.; Wulf, V.; Pelaz, B.; del Pino, P.; Zhao, Y.; de la Fuente, J.; Ruiz de Larramendi, I.; Rojo, T.; Liang, X.-J.; Parak, W. J., The Challenge to Relate the Physicochemical Properties of Colloidal Nanoparticles to Their Cytotoxicity. *Acc. Chem. Res.* **2013,** *46* (3), 743-749.
9. Chen, H. W.; Zou, P.; Connarn, J.; Paholak, H.; Sun, D. X., Intracellular dissociation of a polymer coating from nanoparticles. *Nano Research* **2012,** *5* (11), 815-825.
10. Sée, V.; Free, P.; Cesbron, Y.; Nativo, P.; Shaheen, U.; Rigden, D.; Spiller, D. G.; Fernig, D. G.; White, M. R. H.; Prior, I. A.; Brust, M.; Lounis, B.; Lévy, R., Cathepsin L digestion of nanobioconjugates upon endocytosis. *ACS Nano* **2009,** *3* (9), 2461-2468.
11. Carrillo-Carrion, C.; Bocanegra, A. I.; Arnaiz, B.; Feliu, N.; Zhu, D.; Parak, W. J., Triple-Labeling of Polymer-Coated Quantum Dots and Adsorbed Proteins for Tracing their Fate in Cell Cultures. *ACS Nano* **2019,** *13*, 4631-4639.
12. Sun, X.; Wang, G.; Zhang, H.; Hu, S.; Liu, X.; Tang, J.; Shen, Y., The Blood Clearance Kinetics and Pathway of Polymeric Micelles in Cancer Drug Delivery. *ACS Nano* **2018**.
13. Chen, W. H.; Luo, G. F.; Qiu, W. X.; Lei, Q.; Hong, S.; Wang, S. B.; Zheng, D. W.; Zhu, C. H.; Zeng, X.; Feng, J.; Cheng, S. X.; Zhang, X. Z., Programmed Nanococktail for Intracellular Cascade Reaction Regulating Self-Synergistic Tumor Targeting Therapy. *Small* **2016,** *12* (6), 733-44.
14. Qin, L.; Xue, M.; Wang, W.; Zhu, R.; Wang, S.; Sun, J.; Zhang, R.; Sun, X., The in vitro and in vivo anti-tumor effect of layered double hydroxides nanoparticles as delivery for podophyllotoxin. *Int. J. Pharm.* **2010,** *388* (1-2), 223-30.
15. Feliu, N.; Docter, D.; Heine, M.; Del Pino, P.; Ashraf, S.; Kolosnjaj-Tabi, J.; Macchiarini, P.; Nielsen, P.; Alloyeau, D.; Gazeau, F.; Stauber, R. H.; Parak, W. J., In vivo degeneration and the fate of inorganic nanoparticles. *Chem. Soc. Rev.* **2016,** *45* (9), 2440-57.
16. Kolosnjaj-Tabi, J.; Javed, Y.; Lartigue, L.; Volatron, J.; Elgrabli, D.; Marangon, I.; Pugliese, G.; Caron, B.; Figuerola, A.; Luciani, N.; Pellegrino, T.; Alloyeau, D.; Gazeau, F., The One Year Fate of Iron Oxide Coated Gold Nanoparticles in Mice. *ACS Nano* **2015,** *9* (8), 7925-39.
17. Lartigue, L.; Alloyeau, D.; Kolosnjaj-Tabi, J.; Javed, Y.; Guardia, P.; Riedinger, A.; Pechoux, C.; Pellegrino, T.; Wilhelm, C.; Gazeaut, F., Biodegradation of Iron Oxide Nanocubes: High-Resolution In Situ Monitoring. *Acs Nano* **2013,** *7* (5), 3939-3952.
18. Soenen, S. J.; Parak, W. J.; Rejman, J.; Manshian, B., (Intra)Cellular Stability of Inorganic Nanoparticles: Effects on Cytotoxicity, Particle Functionality, and Biomedical Applications. *Chem. Rev.* **2015,** *115* (5), 2109-2135.
19. Kittler, S.; Greulich, C.; Diendorf, J.; Koller, M.; Epple, M., Toxicity of Silver Nanoparticles Increases during Storage Because of Slow Dissolution under Release of Silver Ions. *Chem. Mater.* **2010,** *22* (16), 4548-4554.
20. Mahon, E.; Hristov, D. R.; Dawson, K. A., Stabilising fluorescent silica nanoparticles against dissolution effects for biological studies. *Chem. Commun.* **2012,** *48* (64), 7970-7972.
21. Van de Walle, A.; Plan Sangnier, A.; Abou-Hassan, A.; Curcio, A.; Hémadi, M.; Menguy, N.; Lalatonne, Y.; Luciani, N.; Wilhelm, C., Biosynthesis of magnetic nanoparticles from nano-degradation products revealed in human stem cells. *Proc. Natl. Acad. Sci.* **2019,** *116*, 4044-4053.
22. Kagan, V. E.; Konduru, N. V.; Feng, W. H.; Allen, B. L.; Conroy, J.; Volkov, Y.; Vlasova, I. I.; Belikova, N. A.; Yanamala, N.; Kapralov, A.; Tyurina, Y. Y.; Shi, J. W.; Kisin, E. R.; Murray, A. R.; Franks, J.; Stolz, D.; Gou, P. P.; Klein-Seetharaman, J.; Fadeel, B.; Star, A.; Shvedova, A. A., Carbon nanotubes degraded by

neutrophil myeloperoxidase induce less pulmonary inflammation. *Nature Nanotechnology* **2010,** *5* (5), 354-359.
23. Javed, Y.; Lartigue, L.; Hugounenq, P.; Quoc Lam, V.; Gossuin, Y.; Bazzi, R.; Wilhelm, C.; Ricolleau, C.; Gazeau, F.; Alloyeau, D., Biodegradation Mechanisms of Iron Oxide Monocrystalline Nanoflowers and Tunable Shield Effect of Gold Coating. *Small* **2014,** *10* (16), 3325-3337.
24. Levy, M.; Luciani, N.; Alloyeau, D.; Elgrabli, D.; Deveaux, V.; Pechoux, C.; Chat, S.; Wang, G.; Vats, N.; Gendron, F.; Factor, C.; Lotersztajn, S.; Luciani, A.; Wilhelm, C.; Gazeau, F., Long term in vivo biotransformation of iron oxide nanoparticles. *Biomaterials* **2011,** *32* (16), 3988-3999.
25. Yu, L.; Chen, Y.; Wu, M.; Cai, X.; Yao, H.; Zhang, L.; Chen, H.; Shi, J., "Manganese Extraction" Strategy Enables Tumor-Sensitive Biodegradability and Theranostics of Nanoparticles. *J. Am. Chem. Soc.* **2016,** *138* (31), 9881-94.
26. Zhang, C.; Ni, D.; Liu, Y.; Yao, H.; Bu, W.; Shi, J., Magnesium silicide nanoparticles as a deoxygenation agent for cancer starvation therapy. *Nat Nanotechnol* **2017,** *12* (4), 378-386.
27. Hong, R.; Han, G.; Fernandez, J. M.; Kim, B. J.; Forbes, N. S.; Rotello, V. M., Glutathione-mediated delivery and release using monolayer protected nanoparticle carriers. *J. Am. Chem. Soc.* **2006,** *128* (4), 1078-1079.
28. Cui, Y.; Dong, H.; Cai, X.; Wang, D.; Li, Y., Mesoporous silica nanoparticles capped with disulfide-linked PEG gatekeepers for glutathione-mediated controlled release. *ACS Appl Mater Interfaces* **2012,** *4* (6), 3177-83.
29. Kim, H.; Kim, S.; Park, C.; Lee, H.; Park, H. J.; Kim, C., Glutathione-induced intracellular release of guests from mesoporous silica nanocontainers with cyclodextrin gatekeepers. *Adv. Mater.* **2010,** *22* (38), 4280-3.
30. Kreyling, W. G.; Abdelmonem, A. M.; Ali, Z.; Alves, F.; Geiser, M.; Haberl, N.; Hartmann, R.; Hirn, S.; de Aberasturi, D. J.; Kantner, K.; Khadem-Saba, G.; Montenegro, J. M.; Rejman, J.; Rojo, T.; de Larramendi, I. R.; Ufartes, R.; Wenk, A.; Parak, W. J., In vivo integrity of polymer-coated gold nanoparticles. *Nature Nanotechnol* **2015,** *10* (7), 619-623.
31. Zhu, L.; Pelaz, B.; Chakraborty, I.; Parak, W. J., Investigating possible enzymatic degradation on polymer shells around inorganic nanoparticles. *Int. J. Mol. Sci.* **2019,** *20*, 935.
32. Lunov, O.; Syrovets, T.; Rocker, C.; Tron, K.; Nienhaus, G. U.; Rasche, V.; Mailander, V.; Landfester, K.; Simmet, T., Lysosomal degradation of the carboxydextran shell of coated superparamagnetic iron oxide nanoparticles and the fate of professional phagocytes. *Biomaterials* **2010,** *31* (34), 9015-9022.
33. de la Rica, R.; Aili, D.; Stevens, M. M., Enzyme-responsive nanoparticles for drug release and diagnostics. *Adv. Drug Del. Rev.* **2012,** *64* (11), 967-978.
34. Callmann, C. E.; Barback, C. V.; Thompson, M. P.; Hall, D. J.; Mattrey, R. F.; Gianneschi, N. C., Therapeutic Enzyme-Responsive Nanoparticles for Targeted Delivery and Accumulation in Tumors. *Adv. Mater.* **2015,** *27* (31), 4611-5.
35. Li, Y.; Liu, G.; Wang, X.; Hu, J.; Liu, S., Enzyme-Responsive Polymeric Vesicles for Bacterial-Strain-Selective Delivery of Antimicrobial Agents. *Angew. Chem. Int. Ed. Engl.* **2016,** *55* (5), 1760-4.
36. Popat, A.; Ross, B. P.; Liu, J.; Jambhrunkar, S.; Kleitz, F.; Qiao, S. Z., Enzyme-Responsive Controlled Release of Covalently Bound Prodrug from Functional Mesoporous Silica Nanospheres. *Angew. Chem. Int. Ed.* **2012,** *51* (50), 12486-12489.
37. Bargheer, D.; Nielsen, J.; Gebel, G.; Heine, M.; Salmen, S. C.; Stauber, R.; Weller, H.; Heeren, J.; Nielsen, P., The fate of a designed protein corona on nanoparticles in vitro and in vivo. *Beilstein Journal of Nanotechnology* **2015,** *6*, 36-46.
38. Llop, J.; Jiang, P.; Marradi, M.; Gomez-Vallejo, V.; Echeverria, M.; Yu, S.; Puigivila, M.; Baz, Z.; Szczupak, B.; Perez-Campana, C.; Mao, Z.; Gao, C.; Moya, S. E., Visualisation of dual radiolabelled poly(lactide-co-glycolide) nanoparticle degradation in vivo using energy-discriminant SPECT. *J. Mater. Chem. B* **2015,** *3* (30), 6293-6300.

39. Bertoli, F.; Garry, D.; Monopoli, M. P.; Salvati, A.; Dawson, K. A., The Intracellular Destiny of the Protein Corona: A Study on its Cellular Internalization and Evolution. *ACS Nano* **2016,** *10*, 10471 - 10479.
40. Casals, E.; Pfaller, T.; Duschl, A.; Oostingh, G. J.; Puntes, V. F., Time Evolution of the Nanoparticle Protein Corona. *ACS Nano* **2010,** *4* (7), 3623-3632.
41. Tenzer, S.; Docter, D.; Kuharev, J.; Musyanovych, A.; Fetz, V.; Hecht, R.; Schlenk, F.; Fischer, D.; Kiouptsi, K.; Reinhardt, C.; Landfester, K.; Schild, H.; Maskos, M.; Knauer, S. K.; Stauber, R. H., Rapid formation of plasma protein corona critically affects nanoparticle pathophysiology. *Nature Nanotechnology* **2013,** *8* (10), 772-U1000.
42. Albanese, A.; Walkey, C. D.; Olsen, J. B.; Guo, H.; Emili, A.; Chan, W. C. W., Secreted Biomolecules Alter the Biological Identity and Cellular Interactions of Nanoparticles. *ACS Nano* **2014,** *8* (6), 5515-5526.
43. Chanana, M.; Rivera Gil, P.; Correa-Duarte, M. A.; Parak, W. J.; Liz-Marzán, L. M., Physicochemical properties of protein-coated gold nanoparticles in biological fluids and cells before and after proteolytic digestion. *Angew. Chem. Int. Ed.* **2013,** *52* (15), 4179-4183.
44. Wang, F. J.; Yu, L.; Monopoli, M. P.; Sandin, P.; Mahon, E.; Salvati, A.; Dawson, K. A., The biomolecular corona is retained during nanoparticle uptake and protects the cells from the damage induced by cationic nanoparticles until degraded in the lysosomes. *Nanomedicine-Nanotechnology Biology And Medicine* **2013,** *9* (8), 1159-1168.
45. Ma, Z.; Bai, J.; Jiang, X., Monitoring of the Enzymatic Degradation of Protein Corona and Evaluating the Accompanying Cytotoxicity of Nanoparticles. *ACS Appl Mater Interfaces* **2015,** *7* (32), 17614-22.
46. Ali, Z.; Abbasi, A. Z.; Zhang, F.; Arosio, P.; Lascialfari, A.; Casula, M. F.; Wenk, A.; Kreyling, W.; Plapper, R.; Seidel, M.; Niessner, R.; Knoll, J.; Seubert, A.; Parak, W. J., Multifunctional Nanoparticles for Dual Imaging. *Anal. Chem.* **2011,** *83* (8), 2877-2882.
47. Escudero, A.; Carrillo-Carrión, C.; Zyuzin, M. V.; Ashraf, S.; Hartmann, R.; Núñez, N. O.; Ocaña, M.; Parak, W. J., Synthesis and functionalization of monodispers near-ultraviolet and visible excitable multifunctional Eu^{3+}, Bi^{3+}:$REVO_4$ nanophosphors for bioimaging and biosensing applications. *Nanoscale* **2016,** *8*, 12221-12236.
48. Bartczak, D.; Nitti, S.; Millar, T. M.; Kanaras, A. G.; , Exocytosis of peptide functionalized gold nanoparticles in endothelial cells. *Nanoscale* **2012**.
49. Kim, J. A.; Aberg, C.; Salvati, A.; Dawson, K. A., Role of cell cycle on the cellular uptake and dilution of nanoparticles in a cell population. *Nature Nanotechnology* **2012,** *7* (1), 62-68.
50. Hartmann, R.; Weidenbach, M.; Neubauer, M.; Fery, A.; Parak, W. J., Stiffness-dependent in vitro uptake and lysosomal acidification of colloidal particles. *Angew. Chem. Int. Ed.* **2015,** *54* (4), 1365-1368.
51. Kim, E.; Osseo-Asare, K., Aqueous stability of thorium and rare earth metals in monazite hydrometallurgy: Eh–pH diagrams for the systems Th–, Ce–, La–, Nd– (PO4)–(SO4)–H2O at 25°C. *Hydrometallurgy* **2012,** *113-114*, 67-78.
52. Rudd, A. L.; Breslin, C. B.; Mansfeld, F., The corrosion protection afforded by rare earth conversion coatings applied to magnesium. *Corros. Sci.* **2000,** *42* (2), 275-288.
53. Hühn, J.; Carrillo-Carrion, C.; Soliman, M. G.; Pfeiffer, C.; Valdeperez, D.; Masood, A.; Chakraborty, I.; Zhu, L.; Gallego, M.; Zhao, Y.; Carril, M.; Feliu, N.; Escudero, A.; Alkilany, A. M.; Pelaz, B.; Pino, P. d.; Parak, W. J., Selected Standard Protocols for the Synthesis, Phase Transfer, and Characterization of Inorganic Colloidal Nanoparticles. *Chem. Mater.* **2017,** *29*, 399−461.
54. Ma, X.; Hartmann, R.; Aberasturi, D. J. d.; Yang, F.; Soenen, S. J. H.; Manshian, B. B.; Franz, J.; Valdeperez, D.; Pelaz, B.; Feliu, N.; Hampp, N.; Riethmüller, C.; Vieker, H.; Frese, N.; Gölzhäuser, A.; Simonich, M.; Tanguay, R. L.; Liang, X.-J.; Parak, W. J., Colloidal Gold Nanoparticles Induce Changes in Cellular and Subcellular Morphology. *ACS Nano* **2017,** *11*, 7807−7820.
55. Jhala, D.; Rather, H.; Vasita, R., Polycaprolactone-chitosan nanofibers influence cell morphology to induce early osteogenic differentiation. *Biomater Sci* **2016,** *4* (11), 1584-1595.

56. Gracz, A. D.; Williamson, I. A.; Roche, K. C.; Johnston, M. J.; Wang, F.; Wang, Y.; Attayek, P. J.; Balowski, J.; Liu, X. F.; Laurenza, R. J.; Gaynor, L. T.; Sims, C. E.; Galanko, J. A.; Li, L.; Allbritton, N. L.; Magness, S. T., A high-throughput platform for stem cell niche co-cultures and downstream gene expression analysis. *Nat. Cell Biol.* **2015,** *17* (3), 340-9.
57. Feliu, N.; Sun, X.; Puebla, R. A. A.; Parak, W. J., Quantitative Particle−Cell Interaction: Some Basic Physicochemical Pitfalls. *Langmuir* **2017,** *33*, 6639−6646.
58. Sun, X.; Gamal, M.; Nold, P.; Said, A.; Chakraborty, I.; Pelaz, B.; Schmied, F.; Pückler, K. v.; Figiel, J.; Zhao, Y.; Brendel, C.; Hassan, M.; Parak, W. J.; Feliu, N., Tracking stem cells and macrophages with gold and iron oxide nanoparticles – The choice of the best suited particles. *Applied Materials Today* **2019,** *15*, 267-279.
59. Summers, H. D.; Brown, M. R.; Holton, M. D.; Tonkin, J. A.; Hondow, N.; Brown, A. P.; Brydson, R.; Rees, P., Quantification of Nanoparticle Dose and Vesicular Inheritance in Proliferating Cells. *Acs Nano* **2013,** *7* (7), 6129-6137.
60. Bourquin, J.; Septiadi, D.; Vanhecke, D.; Balog, S.; Steinmetz, L.; Spuch-Calvar, M.; Taladriz-Blanco, P.; Petri-Fink, A.; Rothen-Rutishauser, B., Reduction of Nanoparticle Load in Cells by Mitosis but Not Exocytosis. *ACS Nano* **2019,** *13*, 77759-7770.
61. Ma, X.; Wu, Y.; Jin, S.; Tian, Y.; Zhang, X.; Zhao, Y.; Yu, L.; Liang, X.-J., Gold Nanoparticles Induce Autophagosome Accumulation through Size-Dependent Nanoparticle Uptake and Lysosome Impairment. *ACS Nano* **2011,** *5* (11), 8629-8639.
62. Sabella, S.; Carney, R. P.; Brunetti, V.; Malvindi, M. A.; Al-Juffali, N.; Vecchio, G.; Janes, S. M.; Bakr, O. M.; Cingolani, R.; Stellacci, F.; Pompa, P. P., A general mechanism for intracellular toxicity of metal-containing nanoparticles. *Nanoscale* **2014,** *6*, 7052-7061.
63. Bourdenx, M.; Daniel, J.; Genin, E.; Soria, F. N.; Blanchard-Desce, M.; Bezard, E.; Dehay, B., Nanoparticles restore lysosomal acidification defects: Implications for Parkinson and other lysosomal-related diseases. *Autophagy* **2016,** *12* (3), 472-83.
64. Meng, H. A.; Xue, M.; Xia, T. A.; Zhao, Y. L.; Tamanoi, F.; Stoddart, J. F.; Zink, J. I.; Nel, A. E., Autonomous in Vitro Anticancer Drug Release from Mesoporous Silica Nanoparticles by pH-Sensitive Nanovalves. *J. Am. Chem. Soc.* **2010,** *132* (36), 12690-12697.
65. Korzeniowska, B.; Woolley, R.; Decourcey, J.; Wencel, D.; Loscher, C. E.; McDonagh, C., Intracellular pH-Sensing Using Core/Shell Silica Nanoparticles. *Journal of Biomedical Nanotechnology* **2014,** *10* (7), 1336-1345.
66. Meng, H. A.; Liong, M.; Xia, T. A.; Li, Z. X.; Ji, Z. X.; Zink, J. I.; Nel, A. E., Engineered Design of Mesoporous Silica Nanoparticles to Deliver Doxorubicin and P-Glycoprotein siRNA to Overcome Drug Resistance in a Cancer Cell Line. *Acs Nano* **2010,** *4* (8), 4539-4550.
67. Domenech, M.; Marrero-Berrios, I.; Torres-Lugo, M.; Rinaldi, C., Lysosomal membrane permeabilization by targeted magnetic nanoparticles in alternating magnetic fields. *ACS Nano* **2013,** *7* (6), 5091-101.
68. Li, W.; Zhao, L.; Wei, T.; Zhao, Y.; Chen, C., The inhibition of death receptor mediated apoptosis through lysosome stabilization following internalization of carboxyfullerene nanoparticles. *Biomaterials* **2011,** *32* (16), 4030-41.
69. Mahmoud, K. A.; Hrapovic, S.; Luong, J. H. T., Picomolar Detection of Protease Using Peptide/Single Walled Carbon Nanotube/Gold Nanoparticle-Modified Electrode. *ACS Nano* **2008,** *2* (5), 1051-1057.
70. Caballero-Díaz, E.; Pfeiffer, C.; Kastl, L.; Rivera-Gil, P.; Simonet, B.; Valcárcel, M.; Jiménez-Lamana, J.; Laborda, F.; Parak, W. J., The Toxicity of Silver Nanoparticles Depends on Their Uptake by Cells and Thus on Their Surface Chemistry. *Part. Part. Syst. Char.* **2013,** *30* (12), 1079-1085.
71. Loza, K.; Diendorf, J.; Greulich, C.; Ruiz-Gonzales, L.; Gonzalez-Calbet, J. M.; Vallet-Regi, M.; Koeller, M.; Epple, M., The dissolution and biological effect of silver nanoparticles in biological media. *J. Mater. Chem. B* **2014,** *2*, 1634-1643.

72. Loza, K.; Epple, M., Silver nanoparticles in complex media: an easy procedure to discriminate between metallic silver nanoparticles, reprecipitated silver chloride, and dissolved silver species. *RSC Advances* **2018,** *8* (43), 24386-24391.